J. Meas. Sci. Instrum., 2024, 15(1): 95-104.
DOI: 10.62756/jmsi.1674-8042.2024010
http://jmsi.publish.founderss.cn/
jmsi@nuc.edu.cn

Three-dimensional electric field sensor with low inter-axis coupling

ZHAO Zhengang[1,2], LI Yitan[1], YANG Xuanyi[1], LUO Chuan[1*]

1. Faculty of Information Engineering and Automation, Kunming University of Science and Technology, Kunming 650500, China;
2. Yunnan Key Laboratory of Green Energy, Electric Power Measurement Digitalization, Control and Protection, Kunming 650500, China

***Corresponding author:** LUO Chuan (luochuan@kust.edu.cn)

Received: October 26, 2023 **Revised:** January 10, 2024 **Accepted:** Feburary 8, 2024

Abstract: When three-dimensional electric field sensor (3D EFS) with orthogonally arranged capacitive-type sensing units is used to measure space electric fields, measurement accuracy is liable to be affected by the coupling effect between axes. In this study, an electric field shielding electrode was proposed to reduce the interaxial coupling effect in 3D EFS and improve the measurement accuracy. Firstly, the multiphysics field simulation software was used to construct an electric field model. Then, the capacitive-type sensing units of the 3D EFS with shielding electrode was developed by simulation results. Finally, an arbitrary angle test platform was set up to experimentally test the 3D EFS with shielding electrodes and the 3D EFS without shielding electrodes. The experimental results showed the measurement deviation of the 3D EFS with shielding electrodes was within 3.2%, which was 12% lower than that of the 3D EFS without shielding electrodes. It can be concluded that the 3D EFS based on the electric field shielding structure can make the decoupling matrix more reliable and reduce the measurement deviation of space electric field.

Key words: capacitive-type electric field sensor (EFS); 3D electric field; simulation analysis; inter-axis coupling; electric field shielding

0 Introduction

Electric field is widely distributed in many fields such as marine, meteorology, electric power[1-4]. The electric field signal detection plays a vital role in safety, security and scientific research[5-7]. The accurate measurement of electric field is beneficial to understanding the spatial characteristics of electric field, such as strength, direction and gradient. Based on this, engineers can optimize the structure, layout and insulation design of power equipment and systems[8-10], and meteorologist s can obtain accurate data on weather forecasting and climate research so as to better understand the spatial characteristics of lightning and thunderstorm activities[11]. In addition, electric field data can be used to verify the accuracy and reliability of electric field simulations[12].

Orthogonally arranged sensing units in three different dimensions enable the measurement of space electric fields. However, the measurement accuracy will be affected by the inter-axis coupling of three-dimensional electric field sensor (3D EFS). To solve this problem, many scholars have conducted a series of studies on the structural design and signal processing of 3D EFS. Wen et al.[13] arrange three micro-electromechanical systems (MEMS) detection units on a non-collinear plane, electric field measurement deviation after decoupling output signal is within 10.2%. Ling et al.[14] arranged three MEMS sensing units orthogonally, and at the same time cooperated with differential circuit to control the measurement deviation of space electric field within 7.13%. However, the MEMS electric field sensors with micro-nano structure have high requirements for packaging process. The effective output signals of MEMS electric field sensors are weak and susceptible to substrate noise interference. In addition, the small sensing area of MEMS sensor requires an external excitation signal, which increases the difficulty in designing sensors. Compared with MEMS electric field sensors, PCB copper-clad laminates only require glue making, gluing, pressing and shearing. Since the large sensing area of PCB electrodes eliminates the need to design external excitation circuits, the output effective signal is large and has better anti-interference capability. Li et al.[15] proposed a decoupled calibration method for 3D EFS based on a genetic algorithm, obtained the optimal decoupled calibration matrix through fitness

function and genetic operator, and solved the problem of matrix inverse complexity, so that the maximum relative error of the synthetic electric field of the 3D EFS was reduced to 1.90%, and the average relative error was reduced to 0.59%. Wu et al.[16] proposed a decoupled calibration method based on a differential evolutionary algorithm to improve the calibration method of 3D spatial EFSs. The algorithm simplifies the complexity and difficulty of the calibration device, and provides a method to calibrate other types of 3D sensors. However, the decoupling calibration cannot eliminate inter-axis coupling from the source. With espect to the measurement of 3D synthetic electric field, Liu et al.[17] developed a measurement method based on a field mill EFS and used unidirectional motion to obtain a 3D field mill structure with a 3D component of the electric field vector. Theoretical deductive analysis, numerical simulation and prototype experiment verified the feasibility of the structure, and the deviation between the test result and the theoretical value was less than 6.79%.

To weaken the interferences of the sensing units themselves between the sensing units of 3D EFS and on the measurement accuracy of space electric field, this study used PCB electrodes as the detection unit of 3D sensor and analyzed the influence of different arrangements of sensing units on the electric field. According to the surface electric field in the test, a shielding scheme was designed for the link that interferes with measurement accuracy. The parameter settings of the shielding electrode was constructed through finite element simulation software to build the induction-shielding model, the structural parameters of the shielding electrode were scanned parametrically to provide a reference for the production of the shielding motor, and thus a 3D EFS was developed. Finally, we built a sensor calibration test platform, calculate the decoupling matrix through the calibration curve, and tested the measurement accuracy of the sensor at different angles.

1 Basic theory

1.1 Measurement principle of 3D EFS

When a conductor is placed in an electric field, positive and negative charges are rearranged on the conductor surface. The relationship between the charge density on the conductor surface and the electric field strength is

$$E=\frac{\sigma}{\varepsilon_0}, \tag{1}$$

where E is the electric field strength, σ is the surface charge density of the conductor, and ε_0 is the vacuum dielectric constant. Under the action of an external electric field, the electrode induces a charge to generate a voltage, and the voltage signal is measured from both sides of the capacitor.

The PCB electrodes is placed into the electric field, consisting of orthogonal copper electrodes and polytetrafluoroethylene (FR-4) filling, as shown in Fig.1. The surface induced charges form an induced electric field E_1 between two copper electrodes. The PCB sensing unit can be equated to a voltage source with an intrinsic capacitance C_{intri} and voltage difference $U_{\text{dif}}(t)$. The field strength of the external electric field can be obtained by measuring the voltage difference $U_{\text{M}}(t)$.

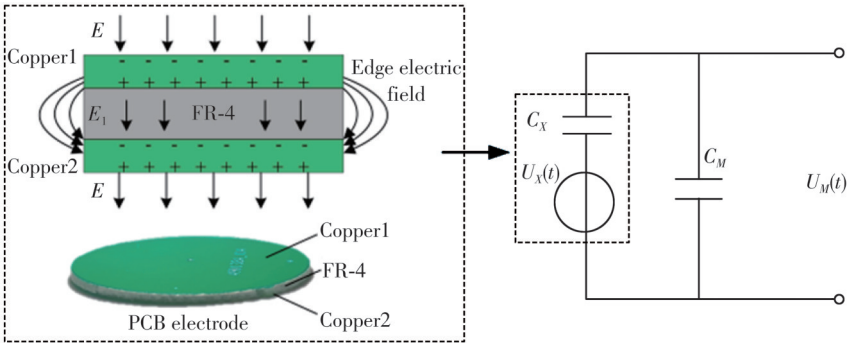

Fig. 1 Equivalent circuit diagram of 3D EFS measurement

When the sensing unit is connected in parallel with a capacitor C_{M} as shown in Fig.1, the relationship between the output signal and the induced charge can be expressed as

$$U_{\text{M}}(t)=U(t)=\frac{Q(t)}{C}, \tag{2}$$

where $U(t)$ is the induced output voltage, $Q(t)$ is the induced charge, $C=C_{\text{M}}+C_{\text{intri}}$ is the parallel measurement capacitance, and C_{X} is the intrinsic capacitance of the induced electrode, which can be express as

$$C_{\text{X}}=\frac{\varepsilon S}{d}, \tag{3}$$

where $\varepsilon=\varepsilon_{\text{r}}\varepsilon_0$ is the relative permittivity of the filling material; S is the direct area of above and below the

electrode, and d is the spacing between the above and below the electrode.

The induced charge is calculatd by

$$Q(t)=\int \sigma \mathrm{d}S=\varepsilon E(t)S. \tag{4}$$

From Eqs. (2) — (4), the output value of the induced voltage can be obtained as

$$U(t)=\frac{\varepsilon_r\varepsilon_0 E(t)S}{C_{\text{intri}}+C_{\text{M}}}. \tag{5}$$

1.2 Analysis of distortion

The electrode is placed in the space electric field, as shown in Fig.2.

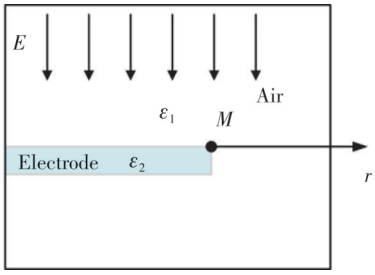

Fig. 2 Edge effect model

When the charge distribution on the probe's surface ceases to change, the potential distribution of the external electric field satisfies the Laplace's equation as

$$\nabla^2 U=0. \tag{6}$$

The edge point of the electrode is selected as the origin of polar coordinate system, namely M point, the electric field decreases in the form of a power function along the polar radius as[18]

$$E=\frac{a}{r^{1-n}}, \tag{7}$$

where r is the distance from point M; α is the parameter associated with the boundary conditions; and n can be expressed in terms of the relative dielectric constant and calculated as

$$n=\frac{2}{\pi}\arccos\sqrt{\frac{1}{2}\frac{\varepsilon_1}{\varepsilon_1+\varepsilon_2}}=\frac{2}{3}, \tag{8}$$

where ε_2 denotes the relative dielectric constant of the electrode, and ε_1 is the relative dielectric constant of air. Therefore, Eq. (7) can be rewritten as

$$E=\frac{a}{r^{1/3}}. \tag{9}$$

Two shapes of electrodes were modeled in the multiphysics field simulation software to study the effect of the electric field induced by the electrodes on the space electric field. The diameter of the arc electrode and the width of the flat electrode are 20 mm, and the electrodes are made of copper. The frequency of the space electric field is 50 Hz and the field strength is 1 kV·m^{-1}. The electric field on the electrode surface is shown in Fig.3.

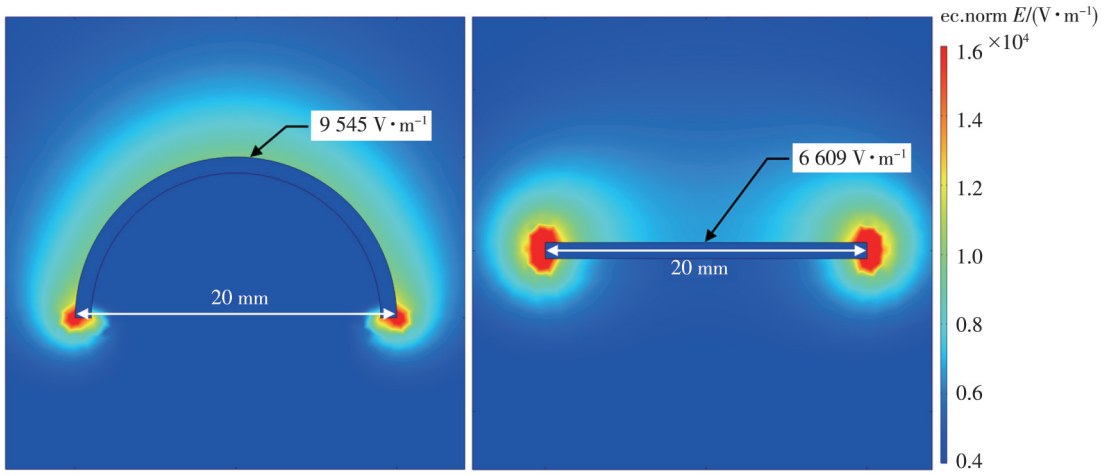

Fig. 3 Electric field distortions caused by two shapes of electrodes

Comparing the electric field modulus at the center of the upper surface of the two electrodes, the electric field modulus on the arc electrode and the flat electrode are 9 545 V·m^{-1} and 6 609 V·m^{-1}, respectively. The distortion of the electric field on the arc electrode is greater than that of the flat electrode.

2 Design of shielding electrode

It is necessary to design a structure that shields the edge effect of the sensing unit to enable a uniform distribution of the electric field on the surface of the sensing unit. For 3D EFS, the edge effect causes the sensing units to interfere with each other in different directions, there by producing an inter-axis coupling effect.

2.1 Edge effect of sensing unit

Two types of PCB sensing unit models were

constructed using multiphysics field simulation software. Fig.4(a) shows the PCB sensing unit without shielding electrode, which is made of FR-4, with a sensing unit radius of R=10 mm and a thickness of 1 mm. Fig.4(b) shows the PCB sensing unit with shielding electrode. The shielding electrode is a square piece of copper with a side length of 30 mm and a thickness of 1 mm, and a circular area with a radius of r_1 is hollowed out in the middle. The circle with radius r_1 is concentric with that with radius R. A 50 Hz, 2.5 kV·m^{-1} alternating electric field was applied in the Z-axis in the air domain, and the direction of the electric field is perpendicular to the surface of the PCB sensing unit. A parameter scanning was performed on r_1 from an initial value of 10 mm to a termination value of 11 mm at a step size of 0.05 mm, and the results are shown in Fig.5.

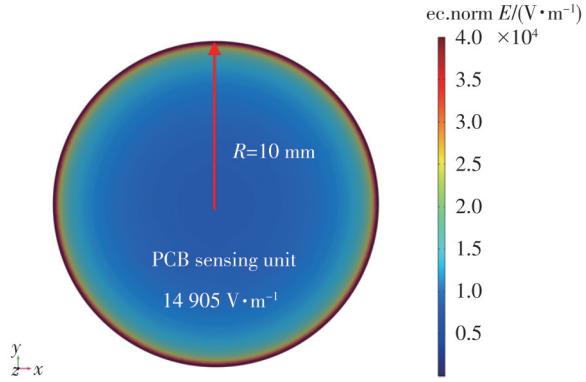

(a) Sensing unit without shielding electrode at f=50 Hz

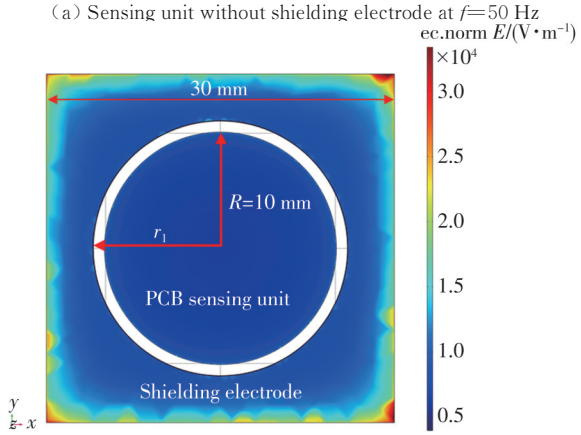

(b) Sensing unit with shielding electrode at r_1=11 mm and at f=50 Hz

Fig. 4 Surface electric field of sensing unit

It can be seen from Figs.4 and 5 that the edge electric field of the sensing unit is much larger than that of the central region, and the average value of the surface electric field modulus is 14 905 V·m^{-1}. After adding the shielding electrode, the electric field on the surface of the sensing unit is uniformly distributed, and the average value of the surface electric field modulus of the sensing unit is positively correlated with parameter r_1. In the production of PCB sensing units with shielding electrodes, the distance between the electrode and the sensing unit can be reduced on the condition that the sensing unit is insulated from the electrode, which can effectively reduce the edge effect of the sensing unit.

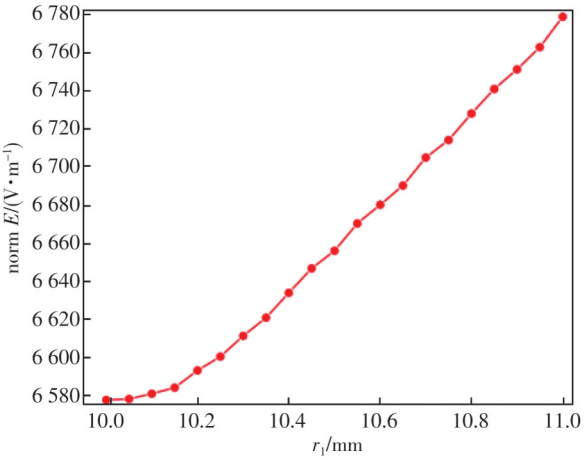

Fig. 5 Variation of electric field modulus of induction electrode surface with parameter r_1

2.2 Coupling effect

The inter-axis coupling model was constructed by multiphysics field simulation software. The parameter scanning of the shielding electrodes was performed, and then the electric field variation on the sensing unit surface was obtained. A PCB sensing unit was put on Z-axis. A 50 Hz, 2.5 kV·m^{-1} alternating field in the Y-axis was constructed in the air domain to represent the field distortion generated by the sensing unit on Y-axis, as shown in Fig.6(a). The PCB sensing unit is made of copper cladded on both sides of FR-4 wafer, with a radius of 10 mm and a thickness of 1 mm. According to the inter-axis coupling model, the average value of the electric field modulus on the surface of the PCB sensing unit is 13 565 V·m^{-1}.

The shielding electrode is put on the PCB sensing unit, as shown in Fig.6(b) and Fig.6(c). The shielding electrode is a square piece of copper with a side length of 30 mm and a circular area with a radius of 10.1 mm hollowed out in the middle. The same alternating electric field as before was applied to investigate the effect of shielding electrode thickness h_1 on the electric field in z-axis. A parameter sacnning was performed on h_1 from an initial value of 1 mm to a termination value of 3 mm with a step size of 0.1 mm h_1. It can be seen that the average value of the electric field modulus on the surface of the sensing unit is negatively correlated with the thickness of the shielding electrode, and the electric field in z-axis coupled to the sensing unit decreases with the increase of the thickness of the shielding

electrode, as shown in Fig.7.

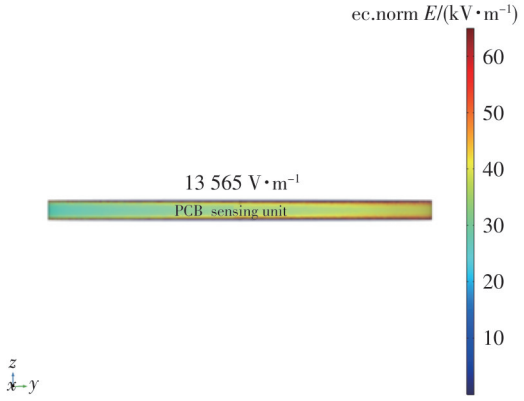

(a) Sensing unit without shielding electrode at f=50 Hz

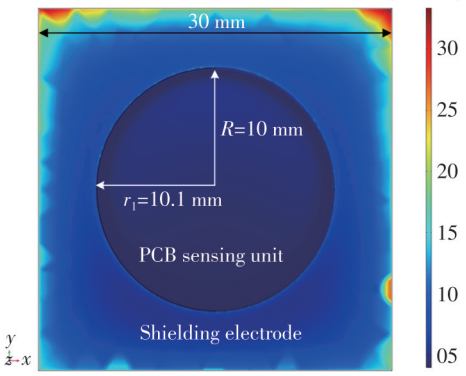

(b) Z-axis view of sensing unit with shielding electrode at h_1=3 mm and f=50 Hz

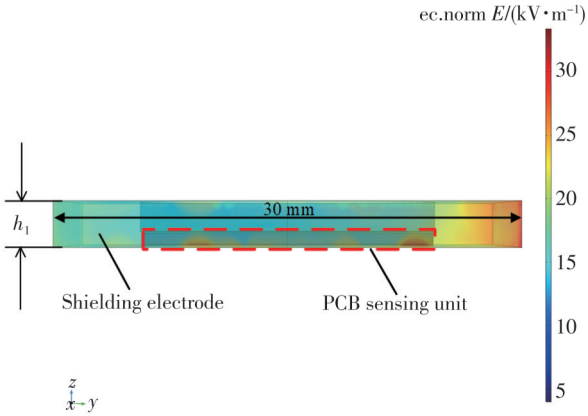

(c) X-axis view of sensing unit with shielding electrode at h_1=3 mm and f=50 Hz

Fig. 6 Surface electric field of electrodes with different structures

2.3 Design of 3D EFS

The PCB sensing units with shielding electrodes were arranged on three adjacent surfaces of the photosensitive resin support, and the three PCB sensing units correspond to X, Y and Z axes in space, respectively. An exploded view of the 3D EFS is shown in Fig.8(a).

The support made of photosensitive resin based on 3D printing technology, as shown in Fig. 8(b). The side length of the support is 30 mm, and a rectangular groove has a depth of 2 mm and a length of 25 mm on support surface. The groove is used to mount the PCB sensing unit while leaving space for soldering and routing the signal wires. The signal lines are buried in the groove to minimize interference with the output signal caused by electric fields.

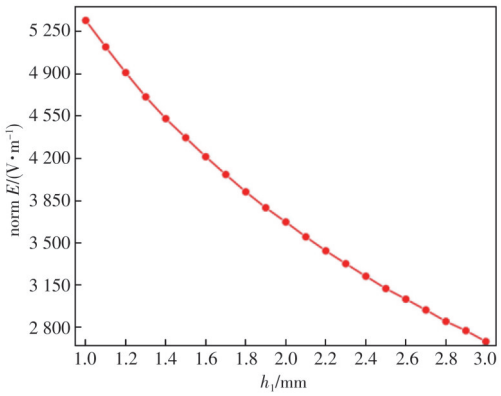

Fig. 7 Variation of electric field modulus of induction electrode surface with parameter h_1

The PCB sensing unit is a rectangular plate with a length of 25 mm and a thickness of 1 mm, as shown in Fig.8(c). A circular copper with a radius of 10 mm is in the center of the upper and lower surfaces, and area out of the circle is made from FR-4 material. The signal line pads are designed outside the circular area.

The shielding electrode is shown in Fig. 8(d). The overall height is 3 mm, the length is 30 mm, and the hollow part is a circle with radius r_1=10.1 mm. The height is 1 mm for the side close to the PCB electrode. There is a 1 mm-thick gap between the PCB electrode and the shielding electrode, which is used to place the starting end of the signal output line to ensure that it is in the shielding area of the shielding electrode to prevent the space electric field from being directly coupled to the signal output end. The shielding electrode is made of copper by computer numerical control (CNC) machining.

2.4 Performance simulation of 3D EFS

The 3D EFS performance model was constructed according to Fig.8.

A 50 Hz, 2.5 kV·m^{-1} alternating electric field is applied in the z-axis in the air domain, and the direction of the electric field is perpendicular to the surface of the z-axis PCB sensing unit with shielding electrode. Let parameters α and β to be the rotation angles of the planes zox and yoz, respectively. The rotation parameters α and β are scanned from an initial value of 0°, the termination value of 45° with a step size of 5°. The electric field modulus of the sensing units surface is the maximum at α=45° and β=45°, as shown in Fig.9.

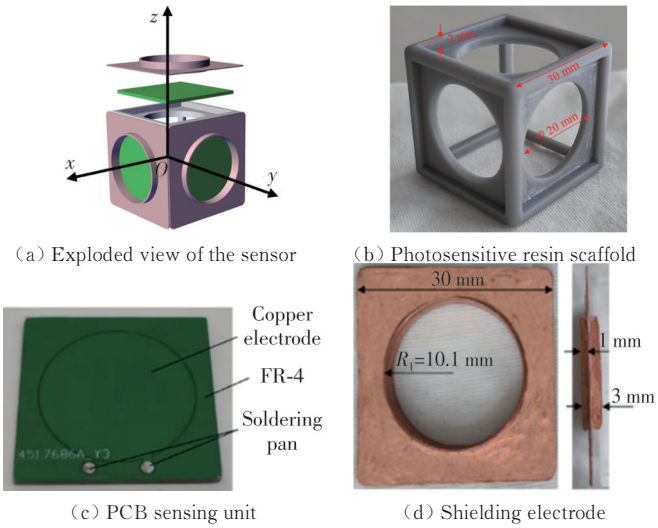

(a) Exploded view of the sensor (b) Photosensitive resin scaffold

(c) PCB sensing unit (d) Shielding electrode

Fig. 8 3D EFS

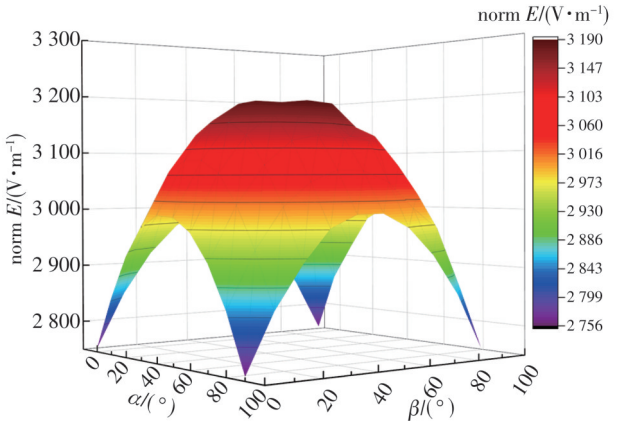

Fig. 9 Variation of electric field modulus of induction electrode surface with parameters α and β

3 Sensor performance test

3.1 Test platform

A parallel plate test platform was used to generate uniformly known field strength[19], as shown in Fig.10. The test platform meets the requirements of the national standard GB/T 12720—1991[20]. The platform consists of a 50 Hz electric field generating device and a signal detection module. The signal detection module is used for detecting the output signals of 3D EFS.

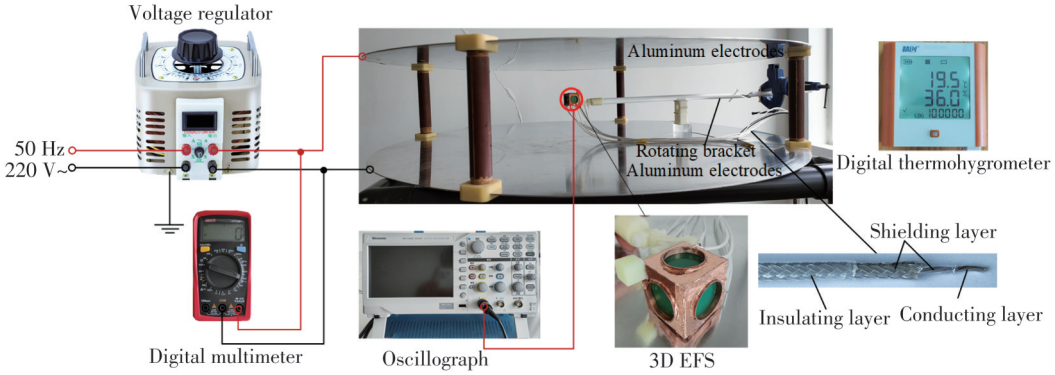

Fig. 10 Calibration test platform

The electric field generating device consists of an AC 0 V—500 V voltage regulator, a digital multimeter with a range of AC 0 V—600 V, and two facing aluminum plates. The multimeter is used to measure the voltage applied to the aluminum plates. Because the charged conductor will produce edge effect, the electric field at the edge is not the standard electric field directly calculated. Here two aluminum plates are designed as a discs with a diameter of 1 m. The distance between the plates is 0.2 m, and four insulating rods are used to ensure that the aluminum plates are insulated from each other. The distance between the pole plate and the wall is greater than two times the plate spacing. When calibrating the sensor, the sensor must be placed in the center of the board to ensure that the measured electric field is the standard given electric field.

The signal detection module consists of a rotating bracket that fixes the 3D EFS, several signal lines, and an oscilloscope. The output signal of the sensor is transmitted to the oscilloscope via the signal line. The signal line is a shielded line, and its structure from inside to outside are signal line layer, insulation layer, metal shield layer, and insulation layer.

3.2 Sensor decoupling calibration

The input-output relationship of the sensor's electrodes in each dimension under the action of coupling factors is[11,12]

$$\boldsymbol{U}_{\text{output}} = \boldsymbol{K}'\boldsymbol{E}_{\text{in}}. \tag{10}$$

In Eq. (10), $\boldsymbol{U}_{\text{output}} = \begin{bmatrix} U_x \\ U_y \\ U_z \end{bmatrix}$ is the sensing voltage output of the sensing unit numbered x, y, z.

$$\boldsymbol{K}' = \boldsymbol{k}\boldsymbol{K}, \text{ with } \boldsymbol{k} = \begin{bmatrix} k_x & 0 & 0 \\ 0 & k_y & 0 \\ 0 & 0 & k_z \end{bmatrix},$$

where k_x, k_y, k_z are the sensitivity coefficients of sensing units perceived under a uniform electric field; and the coupling matrix is

$$\boldsymbol{K}=\begin{bmatrix} K_{xx} & K_{xy} & K_{xz} \\ K_{yx} & K_{yy} & K_{yz} \\ K_{zx} & K_{zy} & K_{zz} \end{bmatrix}, \tag{11}$$

where $K_{iq}(i,\ q=x,\ y,\ z)$ is the coupling sensitivity coefficient of the sensing unit in the i-direction to the electric field in the q-direction.

$\boldsymbol{E}_{\text{in}}=\begin{bmatrix} E_X \\ E_Y \\ E_Z \end{bmatrix}$ is the input of an external electric field.

From Eq. (10) and Eq. (11), the external electric field can be is measured by

$$\boldsymbol{E}_{\text{in}}=(\boldsymbol{K}')^{-1}\boldsymbol{U}_{\text{output}}. \tag{12}$$

The decoupling matrix is

$$\boldsymbol{S}=\begin{bmatrix} k_x K_{xx} & k_x K_{xy} & k_x K_{xz} \\ k_y K_{yx} & k_y K_{yy} & k_y K_{yz} \\ k_z K_{zx} & k_z K_{zy} & k_z K_{zz} \end{bmatrix}^{-1}. \tag{13}$$

Decoupling calibration of 3D EFSs without shielding electrodes and with shielding electrodes was performed at an ambient humidity within 43.9%[21]. The regulator applied an industrial frequency voltage to the pole plate from 0 V to 500 V at a step size of 50 V. Repeating the calibration three times in three dimensions respectively and then averaging them, we obtained the calibration curves in three dimensions, as shown in Figs.11 and 12. The plots (a), (b) and (c) correspond to the outputs when the sensing unit is facing the electric field in the x, y and z directions.

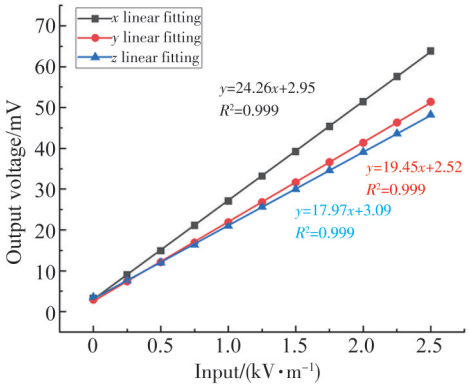

(a) x face up

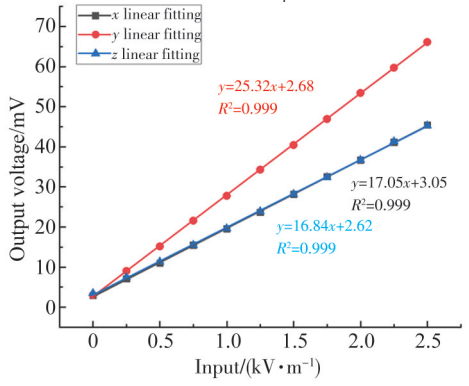

(b) y face up

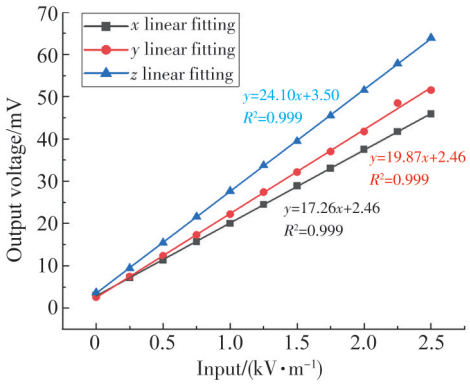

(c) z face up

Fig. 11 Calibration curves of 3D EFS without shielding electrode

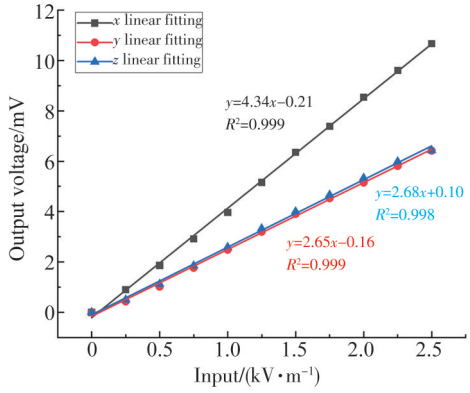

(a) x face up

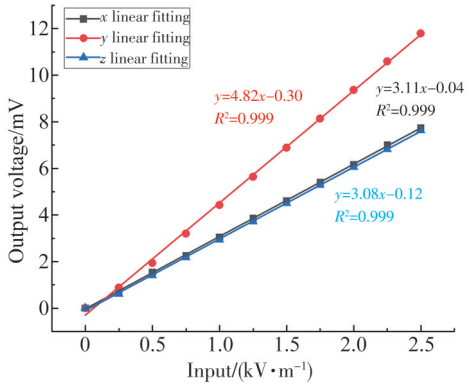

(b) y face up

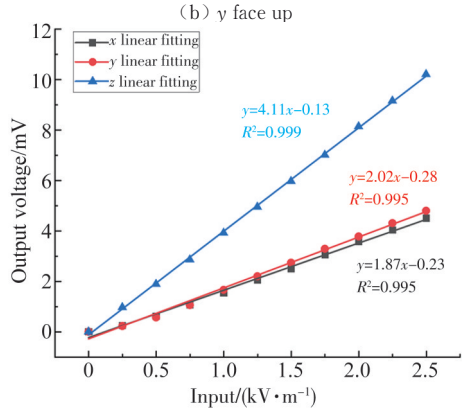

(c) z face up

Fig. 12 Calibration curves of 3D EFS with shielding electrode

The 3D EFS without shielding electrode is shown in Fig.11(a), (b), (c), and the decoupling matrix is derived

from Eq. (13).

$$\boldsymbol{S}_1=\begin{bmatrix}24.26 & 17.05 & 17.26\\ 19.45 & 25.32 & 19.87\\ 17.97 & 16.84 & 24.10\end{bmatrix}^{-1}=\begin{bmatrix}0.11 & -0.05 & -0.04\\ -0.04 & 0.11 & -0.06\\ -0.05 & -0.04 & 0.11\end{bmatrix}.$$

For the 3D EFS with shielding electrode as shown in Fig. 12 (a), (b) and (c), and the decoupling matrix is derived from Eq. (13).

$$\boldsymbol{S}_2=\begin{bmatrix}4.34 & 3.11 & 1.87\\ 2.65 & 4.82 & 2.02\\ 2.68 & 3.08 & 4.11\end{bmatrix}^{-1}=\begin{bmatrix}0.41 & -0.21 & -0.08\\ -0.17 & 0.39 & -0.11\\ -0.14 & -0.15 & 0.38\end{bmatrix}.$$

3.3 Laboratory test

When applying voltages 250 V and 500 V to the aluminum plates of the calibration test rig, respectively, we can get standard electric fields with E of 1.25 kV·m^{-1} and 2.5 kV·m^{-1}, respectively. When adjusting the sensor, its rotation angle was jointly determined by rotation angle α on zox plane and β on yoz plane, as shown in Fig. 13. Finally, the output voltages of the sensor in three axes were measured, and thus the synthetic electric field strength and measurement deviation can be calculated.

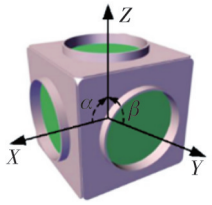

Fig. 13 Rotation angle of sensor

The output vlotages, calculated electric field strengths and deviations of the two EFSs at different angles are shown in Table 1 and Table 2. The deviation is expressed as the ratio of the difference between the applied and calculated electric field strengths to the applied electric field strength.

Table 1 3D EFS with unshielding electrode

Angle/(°)	Applied electric field/(kV·m^{-1})	Output voltage/mV			Calculated electric field/(kV·m^{-1})	Deviation/%
		x	y	z		
α=0, β=45	1.25	29.60	39.62	37.35	1.42	13.6
	2.50	59.89	79.48	75.42	2.83	13.2
α=45, β=0	1.25	30.51	30.69	33.57	1.06	15.2
	2.50	62.72	62.23	67.66	2.13	14.8
α=45, β=45	1.25	35.57	42.62	37.23	1.23	1.6
	2.50	73.61	85.86	75.20	2.43	2.8

Table 2 3D EFS with shielding electrode

Angle/(°)	Applied electric field/(kV·m^{-1})	Output voltage/mV			Calculated electric field/(kV·m^{-1})	Deviation/%
		x	y	z		
α=0, β=45	1.25	4.93	6.54	6.51	1.28	2.4
	2.50	9.84	13.04	13.06	2.57	2.8
α=45, β=0	1.25	6.12	4.67	6.10	1.29	3.2
	2.50	12.75	10.49	12.36	2.50	0
α=45, β=45	1.25	6.72	6.72	6.81	1.26	0.8
	2.50	13.66	13.78	13.74	2.55	2.0

It can be seen that the output voltage of the 3D EFS without shielding electrode in 3D space is larger than that of the 3D EFS with shielding electrode. Due to the edge effect of the electrode, the inter-axis coupling interference to the sensing unit in orthogonal direction appears from edge electric field. The measurement deviation of the 3D EFS without shielding electrode is within 15.2%. The designed EFS overcomes the interference signal coupled to the sensing electrode, so that the measurement deviation of the space electric field is within 3.2%. The deviation may be related to the introduction of the rotating rod and the degree of consistency of the three sensing units in the production process.

4 Conclusions

This paper presents a 3D EFS with shielding electrodes to deal with the effects of interaxial coupling effects. Aiming at the edge effect existing in the plate electrode and the coupling interference, the finite element simulation model was constructed, and parameter scanning of the shielding electrode structure was carried out. The degree of interference to the sensing unit is positively correlated with the distance between the shielding electrode and the induction electrode and negatively correlated with the height of the shielding electrode. Based on the parameter scanning results the prototype production of the 3D EFS was completed. Then, the developed 3D EFS with

shielding electrode and the 3D EFS without shielding electrode into the standard electric field for calibration, and the calibration results was used to calculate the decoupling matrix. Finally, rotating the two EFSs into the test platform at the same angle, the test results were compared. The experimental results showed that the measurement deviation of 3D EFS with shielding electrodes was within 3.2%, which is 12% higher than that of the 3D EFS without shielding electrodes.

Acknowledgement

This work was supported by National Natural Science Foundation of China (No.62162035).

Declaration of conflicting interests

The authors have no conflict of interests related to this publication.

References

[1] HU Z, PENG Y, GUO D, et al. Flexible composite Ag-AgNWs-CF as low noise marine electric field sensor. Composites Part A: Applied Science and Manufacturing, 2022, 152: 106711.

[2] HU Z, HE T, LI W, et al. Controllable 3D flower-like Ag-CF electrodes as flexible marine electric field sensors with high stability. Inorganic Chemistry, 2023, 62(8): 3541-3554.

[3] YANG X, XING H, XU W, et al. A moving path tracking method of the thunderstorm cloud based on the three-dimensional atmospheric electric field apparatus. Journal of Sensors, 2021, 2021: 1-13.

[4] SHENG W Q, LI G, LI Y Z, et al. Comprehensive simulation of snow crystal deposition and electric field characteristics of composite sheath improved porcelain cantilever insulator in a wind and snow enviroment. Journal of Measurement Science and Instrumentation, 2022, 13(14): 379-389.

[5] XING H, HE G, JI X. Analysis on electric field based on three-dimensional atmospheric electric field apparatus. Journal of Electrical Engineering & Technology, 2018, 13(4): 1697-1704.

[6] WANG H, ZHUANG C, ZENG R, et al. Transient voltage measurements for overhead transmission lines and substations by metal-free and contactless integrated electro-optic field sensors. IEEE Transactions on Industrial Electronics, 2018, 66(1): 571-579.

[7] SUO C, ZHAO J, ZHANG W, et al. Research on UAV three-phase transmission line tracking and localization method based on electric field sensor array. Sensors, 2021, 21(24): 8400.

[8] HAO J P, LIU S T, YANG K, et al. The Technology of Space Electric Field Detection of Deteriorated Insulator Strings Based on Multi Rotor UAV//Journal of Physics: Conference Series, 2022, 2215(1): 012022.

[9] GHASEMZADEH M R, FAGHIHI F, MOZAFARI S B. FEM analysis of elliptical void in insulator of GIS compartment based on electric field distribution. Electric Power Systems Research, 2023, 220: 109261.

[10] LI X, YANG L, YIN Q, et al. Lightning Risk Warning Method Using Atmospheric Electric Field Based on EEWT-ASG and Morpho. Atmosphere, 2023, 14(6): 1002.

[11] ZHU H, HAN Z, LIU C, et al. Simulation analysis of synthetic electric field of UHV transmission line under mountain fire condition. Electric Power Systems Research, 2023, 222: 109490.

[12] WEN X, PENG C, FANG D. Measuring method of three-dimensional atmospheric electric field based on coplanar decoupling structure. Journal of Electronics & Information Technology, 2014, 36(10): 2504-2508.

[13] LING B, PENG C, Ren R, et al. MEMS-based three-dimensional electric field sensor with low cross-axis coupling interference. Journal of Electronics & Information Technology, 2018, 40(8): 1934-1940.

[14] LI B, PENG C, LING B, et al. The Decoupling Calibration Method Based on Genetic Algorithm of Three-Dimensional Electric Field Sensor. Journal of Electronics & Information Technology, 2017, 39(9): 2252-2258.

[15] WU G F, CUI Y, LIU H, et al. Decoupling calibration method of 3D electric field sensor based on differential evolution algorithm. Transactions of China Electrotechnical Society, 2021, 36(19): 3993-4001.

[16] LIU C, YUAN H, LV J, et al. A Sensor for 3-D component measurement of synthetic electric field vector in HVDC transmission lines using unidirectional motion. IEEE Transactions on Instrumentation and Measurement, 2022, 72: 1-10.

[17] WANG J X, LI H, WANG Z H, et al. Research on electric field distortion at the edge of metallized film capacitor electrode, High Voltage Apparatus, 2022, 58: 29-36.

[18] LUO F S, HE Y H, ZHANG W H, et al. Calibration method of electric field. Chinese Journal of Space Science, 2007, 27(3): 223-226.

[19] Xi'an High Voltage Apparatus Research Institute. Measurement of power-frequency electric fields: GB/T 12720-1991. The State Bureau of Quality and Technical Supervision, 1991.

[20] LAN X S, DING D W, WANG Z G, et al. Study on the effects of the environmental humidity on the accuracy of power frequency electric field measurement equipment in laboratory and improvement measures. High Voltage Apparatus, 2018, 54(2): 246-251.

低轴间耦合的三维电场传感器

赵振刚[1,2], 李宜锑[1], 杨玄奕[1], 罗　川[1*]

1. 昆明理工大学 信息工程与自动化学院, 云南 昆明 650500;
2. 云南省绿色能源与数字电力量测及控保重点实验室, 云南 昆明 650500

摘　要: 使用正交排列的电容式传感单元的三维电场传感器(Three-dimensional electric field sensor, 3D EFS)测量空间电场时, 轴间耦合效应会严重影响EFS的测量精度。为此, 提出了一种电场屏蔽电极, 以降低3D EFS的轴间耦合效应, 提高测量精度。首先, 利用多物理场仿真软件构建电场分布模型。其次, 根据仿真结果建立带屏蔽电极的3D EFS电容式传感单元的屏蔽电极模型。最后, 建立任意角度的测试平台, 将带有屏蔽电极的3D EFS和无屏蔽电极的3D EFS进行实验对比。结果显示, 有屏蔽电极的3D EFS的测量偏差在3.2% 以内, 比无屏蔽电极的3D EFS的测量偏差减少12%。因此, 所设计的基于电场屏蔽结构的3D EFS可以使解耦矩阵更加可靠, 有效降低空间电场测量偏差。

关键词: 电容式电场传感器; 空间电场; 仿真分析; 轴间耦合; 电场屏蔽

引用格式: ZHAO Zhengang, LI Yitan, YANG Xuanyi, et al. Three-dimensional electric field sensor with low inter-axis coupling. Journal of Measurement Science and Instrumentation, 2024, 15(1): 95-104.